Acta Oceanol. Sin., 2018, Vol. 37, No. 3, P. 31–41
DOI: 10.1007/s13131-018-1198-0
http://www.hyxb.org.cn
E-mail: hyxbe@263.net

Turbulent mixing above the Atlantic Water around the Chukchi Borderland in 2014

ZHONG Wenli[1]*, GUO Guijun[1, 2], ZHAO Jinping[1], LI Tao[1], WANG Xiaoyu[1], MU Longjiang[1, 3]

[1] Key Laboratory of Physical Oceanography, Ocean University of China, Qingdao 266100, China

[2] Center for Ocean and Climate Research, The First Institute of Oceanography, Qingdao 266061, China

[3] Key Laboratory of Research on Marine Hazards Forecasting, National Marine Environmental Forecasting Center, State Oceanic Administration, Beijing 100081, China

Received 9 May 2017; accepted 15 June 2017

Abstract

This study presents an analysis of the CTD data and the turbulent microstructure data collected in 2014, the turbulent mixing environment above the Atlantic Water (AW) around the Chukchi Borderland region is studied. Surface wind becomes more efficient in driving the upper ocean movement along with the rapid decline of sea ice, thus results in a more restless interior of the Arctic Ocean. The turbulent dissipation rate is in the range of 4.60×10^{-10}–3.31×10^{-9} W/kg with a mean value of 1.33×10^{-9} W/kg, while the diapycnal diffusivity is in the range of 1.45×10^{-6}–1.46×10^{-5} m^2/s with a mean value of 4.84×10^{-6} m^2/s in 200–300 m (above the AW). After investigating on the traditional factors (i.e., wind, topography and tides) that may contribute to the turbulent dissipation rate, the results show that the tidal kinetic energy plays a dominating role in the vertical mixing above the AW. Besides, the swing of the Beaufort Gyre (BG) has an impact on the vertical shear of the geostrophic current and may contribute to the regional difference of turbulent mixing. The parameterized method for the double-diffusive convection flux above the AW is validated by the direct turbulent microstructure results.

Key words: Atlantic Water, Chukchi Borderland, turbulent dissipation rate, diapycnal diffusive, surface stress

Citation: Zhong Wenli, Guo Guijun, Zhao Jinping, Li Tao, Wang Xiaoyu, Mu Longjiang. 2018. Turbulent mixing above the Atlantic Water around the Chukchi Borderland in 2014. Acta Oceanologica Sinica, 37(3): 31–41, doi: 10.1007/s13131-018-1198-0

1 Introduction

The Atlantic Water (AW) in the Arctic Ocean which originates from the northern Atlantic Ocean contains a large amount of energy and is the most important heat energy in the Arctic region. Since the 1990s, the Atlantic Water has experienced several warm events, with two warmest signal appeared in 1990 and 2006 in the Fram Strait (Kikuchi et al., 2005; Polyakov et al., 2011). The warm pulse-like signal of 1990 reaches the Chukchi Borderland region (CBR, including Chukchi Rise, Chukchi Gap, Northwind Ridge, Northwind Abyssal Plain and Northwind Gap) around 1999, which results in an increase of ~1°C higher than the climatological record (Carmack et al., 1995; Zhao et al., 2005). Along with the warmer AW is the shoaling depth of the AW which would change the vertical heat flux and further have a great effect on the ocean circulation (Polyakov et al., 2004, 2010, 2012; McLaughlin et al., 2005). However in 2002, the AW in the western Mendeleev Ridge appears be to colder than the AW in the Chukchi Borderland region which indicates that relatively colder AW is transported from upstream area to downstream area (Woodgate et al., 2007). This colder AW flows into the Canada Basin in 2004 in the form of thermohaline intrusion and replaces the relatively warm AW in the western basin gradually (Zhong and Zhao, 2014; Zhong et al., 2015). The AW flows through the Chukchi Borderland region which has a complex topography before it finally flows into the Canada Basin. This region plays a vital role in regulating the heat dissipation of AW and strongly impacts the extension and transport time of the AW, etc. (Shimada et al., 2004). When the AW reaches the Chukchi Rise, it is topographically constrained and one flows around the Chukchi Rise to the northeast and one flows through the southern Chukchi Gap and into the Northwind Ridge Abyssal Plain to the southeast and finally flows into the Beaufort Sea (Shimada et al., 2004; Woodgate et al., 2007; McLaughlin et al., 2009). The different transit distances between these two branches could result in different response timescales in downstream (the Canada Basin) to the upstream variability (Shimada et al., 2004). Owing to the complex topography of the Chukchi Borderland region, the movement and renew rate of parts of the water there are constrained, i.e., the AW in the Northwind Ridge Abyssal Plain has its own relic water properties and a slow update rate (Woodgate et al., 2007). The AW could be upwelled and mixed with the inflowing Pacific Water in the Chukchi Sea Shelf/Slope at the southern Chukchi Borderland region, and thus has an impact on the Arctic's lower halocline (Woodgate et al., 2005).

The double diffusive convection structure forms between the cold and fresh Pacific Water and the warm and salt AW in the western Arctic Ocean (e.g., Padman and Dillon, 1987; Timmermans et al., 2008). This unique vertical structure is a common

Foundation item: The Key Project of Chinese Natural Science Foundation under contract No. 41330960; the National Basic Research Program (973 Program) of China under contract No. 2015CB953902; the Ph D Programs Foundation of Ministry of Education of China under contract No. 20130132110021; the National Natural Science Foundation of China under contract No. 41706211.
*Corresponding author, E-mail: wlzhongouc@ouc.edu.cn

phenomenon around the Arctic Ocean, also appears in the Laptev Sea and the central Arctic Ocean. It has a great effect on the vertical heat transfer of the AW and the maintenance of the cold halocline (Fer, 2009). Before the 1990s, the Arctic Ocean was covered by extensive thick ice and because of this, the transfer of wind energy into the ocean was restricted. The interior Arctic Ocean was relatively quiescent. But the sea ice has experienced a dramatic decline in recent years, especially in the Chukchi Borderland and its adjacent regions where large ice-free area appears in the south of the Chukchi Borderland region in summer. There are several factors that contribute to the northward retreat of sea ice, one of them is the inflowing Pacific Summer Water from the Chukchi Sea (i.e., Shimada et al., 2006). In summer, the ocean surface is exposed under the direct wind forcing in the open water region instead of damping by sea ice, which results in a stronger air-sea interaction (Rainville et al., 2011). In addition, the sea ice motion intensified as the sea ice becomes thinner and less areal coverage (Rainville and Woodgate, 2009; Yang, 2009). An intensification of near-inertial waves was observed which promotes stronger vertical mixing in the ocean interior (Rainville et al., 2011; Dosser et al., 2014; Dosser and Rainville, 2016). This has a potential effect for the heat transfer from AW to the upper layer and if this heat is brought to the surface it would have a big impact on the melting of sea ice (Polyakov et al., 2010; Turner, 2010).

Many studies have shown substantially enhancement of turbulent mixing over rough topography due to the interaction between tides and topography (Padman and Dillon, 1991; D'Asaro and Morison, 1992; Rainville and Winsor, 2008; Lenn et al., 2009), while the basin interior still has a relatively weak turbulent mixing (Fer, 2009; Guthrie et al., 2013; Rippeth et al., 2015). Although the wind-induced near-inertial waves would increase as the decline of sea ice continues, Guthrie et al. (2013) and Rippeth et al. (2015) have shown that the vertical turbulence is insensitive to the sea ice condition at present situation. One of the reasons comes from the melting of sea ice which results in a stronger stratification that depress the propagation of near-inertial waves (Guthrie et al., 2013). However, as the declining trend of sea ice continues, and along with that is the possible release of freshwater by the shifting circulation regime in the Arctic Ocean (Proshutinsky et al., 2009) and the weaker stratification. It is reasonable to assume that the wind-induced near-inertial waves would have greater impact on the interior mixing of the ocean which resulting in an increase and expansion of mixing hotspots (Rippeth et al., 2015).

In this study, the mixing process above the AW around the Chukchi Borderland and its adjacent region was analyzed based on the microstructure data that was collected in the 2014 summer research cruise. The main goal of this study is to reveal the pivotal role of Chukchi Borderland region in regulating the AW vertical heat flux in an AW cooling scenario. We focus on the increase of the wind energy into the ocean by retreating sea ice and the corresponding increase in the vertical mixing. We discuss the double-diffusive convection in the vertical heat transfer of the AW and its regional difference in a cooling scenario. The paper is organized as follows. Section 2 is data and methods. In Section 3, we analyzed the results and the factors that controlling the vertical mixing process above the AW. In Section 4, the laboratory parameterized double-diffusive convection flux above the AW was analyzed and compared with the measured flux from the vertical microstructure profile. Our conclusions and discussion are presented in Section 5.

2 Data and methods

2.1 *Turbulent microstructure data processing*

In August 2014, the research vessel *Xuelong* of China deployed a large survey around the Chukchi Borderland and its adjacent region. Temperature and salinity measurements were carried out at 22 stations over this region and 21 of them has microstructure observations (and 16 of these with the deepest deployed depth over 200 m, Fig. 1a). The Rockland scientific Vertic-

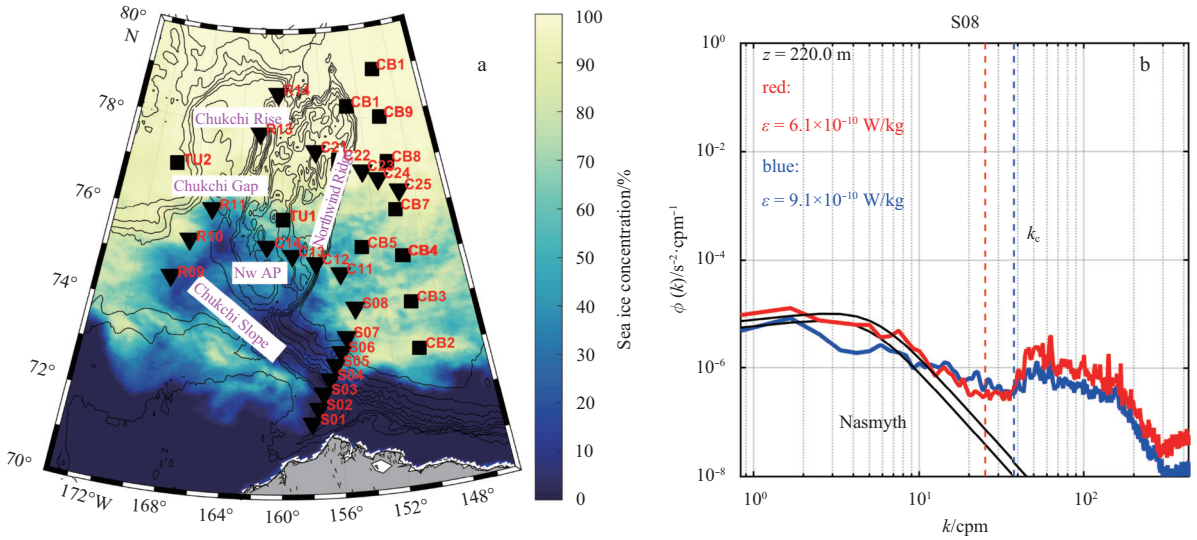

Fig. 1. Stations map and an example of shear spectrum. a. The CTD stations and the mean sea ice condition (AMSR2 data) during the VMP deployment in August 2014. The inverted triangle represents stations that have both CTD and VMP deployment while the square represents stations that have only CTD deployment. The isobaths are shown as black contour, ranging from 50 to 4 000 m with an interval of 500 m in 500–4 000 m and an interval of 50 m in 50–150 m. Nw AP is short for the Northwind Abyssal Plain. b. An example of a shear spectrum observed by a VMP superimposed on the Nasmyth spectrum (black line), where k_c is the integration cut-off wave number.

al Microstructure Profiler (VMP-200) which includes two shear probes, one thermistor and one micro-conductivity probe was used to obtain the microstructure data in a free-fall mode with typical fall speeds of ~0.6 m/s. The shear data above 20 m was removed to exclude anomalous data spikes that susceptible to ship-wake turbulence and post-bottom impact. In isotropic turbulence, the rate of dissipation can be derived from observed turbulent shear data (sampling rate of 512 Hz), i.e., the velocity shear spectra were integrated through an iterative procedure between the higher cut-off wavenumber, the Kolmogoroff wave number $k_S=(2\pi)^{-1}(\varepsilon\upsilon^{-3})^{1/4}$, and the lower bounds at 1 cycle per meter (cpm) and then we derived the turbulent dissipation rate ε as:

$$\varepsilon=\frac{15}{2}\upsilon\overline{\left(\frac{\partial u}{\partial z}\right)^2}=\frac{15}{2}\upsilon\int_0^{\infty}\varphi(k)\mathrm{d}k\approx\frac{15}{2}\upsilon\int_1^{k_S}\varphi(k)\mathrm{d}k,$$

where υ is the kinematic viscosity of seawater. The shear spectrum $\varphi(k)$ in the range below k_c is well consistent with the fitted Nasmyth's universal spectrum (Fig. 1b), indicating small systematic error. Based on the turbulent dissipation rate and buoyancy frequency squared from temperature and salinity, the diapycnal diffusivity can be estimated as

$$K_\rho=\Gamma\varepsilon/N^2,$$

where the mixing efficiency is Γ=0.2 (Osborn, 1980). The above equation is valid when the buoyancy Reynolds number $R_\varepsilon=\varepsilon/(\upsilon N^2)$ falls into the range of $7<R_\varepsilon<100$ (Ivey et al., 2008).

The hydrographic data from the Beaufort Gyre Exploration Project (BGEP) (http://www.whoi.edu/beaufortgyre/) in 2014 is also used to abundant our study area to get an overview of the spatial distribution of the AW over the Chukchi Borderland and its adjacent region.

The ice-ocean stress over the sea-ice covered ocean was calculated based on the sea ice motion vectors data (Tschudi et al., 2016) and the sea ice concentration data (AMSR2, with a horizontal resolution of 6.25 km×6.25 km; Spreen et al., 2008). The wind stress is derived from ERA-Interim 10 m winds from the European Centre for Medium-Range Weather Forecasts (ECMWF) reanalysis, with a horizontal resolution of 0.75°×0.75°(Dee et al., 2011). Using the wind stress and the ice-ocean stress we then calculated the total stress on each grid based on the sea ice concentration as suggested by Yang (2009), i.e.,

$$\vec{\tau}=\alpha\vec{\tau}_{\text{ice-water}}+(1-\alpha)\vec{\tau}_{\text{air-water}},$$

where α is the sea ice concentration, and $\vec{\tau}_{\text{air-water}}=\rho_{\text{air}}C_{\text{d}}|\vec{u}_{\text{s}}|\vec{u}_{\text{s}}$, $\vec{\tau}_{\text{ice-water}}=\rho_{\text{water}}C_{\text{iw}}|(\vec{u}_{\text{ice}}-\vec{u}_{\text{ocean}})|(\vec{u}_{\text{ice}}-\vec{u}_{\text{ocean}})$, $\rho_{\text{air}}=1.25\ \text{kg/m}^3$, $C_{\text{d}}=0.001\ 25$ is the air-water drag coefficient, $\vec{u}_{\text{s}}$ is the wind speed, ρ_{water} is the water density, $C_{\text{iw}}=0.005\ 5$ is the ice-water drag coefficient, $\vec{u}_{\text{ice}}$ and $\vec{u}_{\text{ocean}}$ is the ice motion velocity and surface Ekman current velocity respectively.

2.2 *The tidal kinetic energy*

The Arctic Ocean Dynamics-based Tide Model (AODTM-5) barotropic forward tide model for the Arctic Ocean (Padman and Erofeeva, 2004) is used to calculate the tidal kinetic energy that may contribute to the mixing process. Four major tidal components are consider here: M_2, S_2, K_1 and O_1. The model solving the shallow water equations following Egbert and Erofeeva (2002) with a model outputs in a resolution of 5 km×5 km. The tidal kinetic energy is given by $E_{\text{tk}}=1/2\cdot\rho_{\text{ref}}H(u^2+v^2)$, where ρ_{ref} is the reference density, H is the corresponding model grid depth which shallower than 300 m, $u(v)$ is the model output of the tidal velocity.

2.3 *Vertical shear of geostrophic current*

The Chukchi Borderland and its adjacent region are highly regulated by the Beaufort Gyre (BG). In order to evaluate the impact of BG, the vertical shear of geostrophic current is derived based on the thermal wind equations, i.e., $\overline{S}_{\text{GV}}=g/(f\rho_0)\partial\sigma_\theta/\partial s$ (Kaneko et al., 2012), where f is the Coriolis parameter, ρ_0 is the reference density, σ_θ is the potential density from CTD profiles, s is the distance between two adjacent stations.

3 Mixing above the Atlantic Water and its contributing factors

3.1 *Atlantic Water around the Chukchi Borderland*

The warm AW deepened as it flows further into the Arctic Ocean basin and it is strongly constrained by the topography. The AW diverges into two branches when it flows to the west of the Chukchi Borderland. One branch flows along the periphery of Chukchi Rise, while the other flows across the Chukchi Gap (~1 000 m) into the Chukchi Borderland. The temperature of AW appears to be relatively high in the western and northern Chukchi Borderland with the highest appears in the north-eastern part (>0.85°C). The temperature of AW decreases gradually to the south-eastern part. The average temperature of AW in the western Canada Basin is around 0.79°C with a relatively cold temperature in the east of the Northwind Ridge and the Beaufort Sea (Fig. 2a). Correspondingly, relatively shallow AW appears in the north and south regions while relatively deep AW dominates in the middle region (here the depth of AW is determined by finding the depth with the maximum temperature of AW). The typical depth of AW is more than 460 m over the middle western Canada Basin (Fig. 2b) while it is shallower than 440 m in the northern Chukchi Borderland and the Beaufort Sea.

Here the heat content is defined as $C_{\text{h}}=\rho C_{\text{p}}\Delta TS$, where ρ is density, C_{p} is heat capacity of sea water, $\Delta T=T-T_0$, T is the potential temperature, T_0 is the freezing point temperature and S is the water column height/volume per unit area. It is obvious there is a small heat content value at Sta. TU1 (Fig. 2c). From the temperature and density profile of Sta. TU1, a cold halocline eddy was detected with its core around 200 m depth. This eddy dramatically changes the water properties above the AW. The dynamics of the eddy is not our issue here. We focus on the overall changes of the AW around the Chukchi Borderland and its adjacent regions (Fig. 2c). The heat content (200–600 m) of most stations exceed 8.2 GJ/m^2 except Sta. TU1. One interesting phenomenon to be noticed is that relatively low heat content appears in the western Canada Basin while it is higher in the northern and southern basin. This spatial pattern maybe a result of the transport of warm pulses of AW. Along with the 1990s' anomalously warm AW that reached the southwestern Canada Basin is an inflows of relatively cold AW. And this relatively cold AW dominates the western Canada Basin while later another warm pulse AW follows to the northeastern part of the Northwind Ridge which results in this spatial difference of heat content. The heat content difference between Stas TU2 (in the Chukchi Gap) and

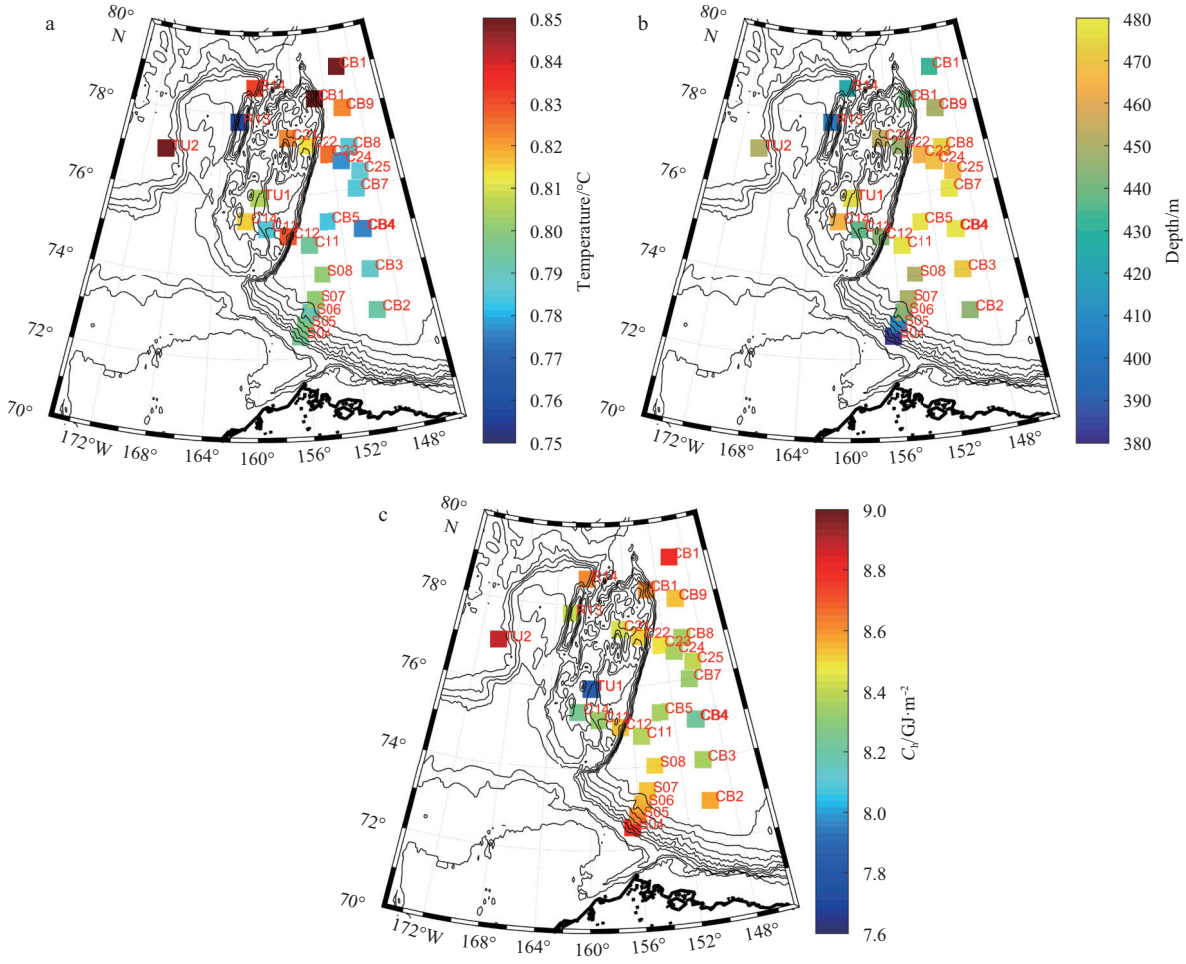

Fig. 2. The maximum temperature of Atlantic Water (a), depth of AW (b) and heat content in 200–600 m (c).

C14 (in the Northwind Abyssal Plain) is ~0.633 GJ/m^3. Assumed the AW boundary current velocity as 1.5 cm/s as an approximation from Stas TU2 to C14 (current velocity refers to Woodgate et al., 2007) and the distance between two stations is 292 km, we then have the flowing time of AW as 225.3 days. Considered a maximum heat flux above the AW to be 1 W/m^2 (in the following part, results will show that the overall heat flux above the AW is below 1 W/m^2), then we would have the total heat loss of AW to be 1×225.3×24×3 600=19.5 (MJ/m^2) which is far more lower than the heat content reduction of 0.633 GJ/m^2. This large discrepancy has two possible explanations. One is that most of the heat energy of AW is transported by the northward branch of AW that flows along the western Chukchi Rise. The other is that Sta. C14 might be not located at the center of the flowing pathway of AW. Constrained by the potential vorticity, the branch of AW that flows across the Chukchi Gap and into the south of Nw AP (along the Chukchi Slope) does not have much water exchange with the interior of Nw AP like Sta. C14. Further investigation is needed to better evaluate the proportion for different branches of AW.

3.2 *Mixing above the AW around the Chukchi Borderland*

According to the obtained microstructure shear data, the turbulent dissipation rate and diapycnal diffusivity were calculated (Figs 3a and b). The vertical section shows a weak mixing below 100 m around the west-southern Canada Basin (relatively small value of the turbulent dissipation rate) comparing with a relatively strong mixing below 100 m around the Chukchi Borderland and the western Canada Basin. The overall turbulent dissipation rate falls in the range of 3.03×10^{-10}–4.98×10^{-9} W/kg while the diapycnal diffusivity is in the range of 1.18×10^{-7}–7.86×10^{-5} m^2/s. The Stas R09 and R11 (water depth <500 m) show a consistent strong mixing in all depth in Section R (here and after, the station name with the initial of "R" is named as Section R). While the mixing at Stas C24 and C25 (located in the western basin) are stronger than that at Stas C23 and C21 (located near Northwind Ridge). Stas R09, R10 and R11 are located at the sea ice edge and during August 1–14 the sea ice was rapid retreating to the northwestern side around the Chukchi Borderland region. Relatively strong surface stress appears at these stations (Fig. 3c). This indicates that strong surface forcing exerts on the upper ocean and that may results in these relatively strong vertical mixing. The diapycnal diffusivity increases dramatically below 300 m (i.e., below the halocline). The main cause of this increase is weaker stratification below the halocline. The order of diapycnal diffusivity could reach 10^{-5} m^2/s and it is increasing toward the AW core which indicates an increase of the vertical upward of heat flux.

Studies have shown an increase of surface stress as the sea ice retreat (Martin et al., 2014; Tsamados et al., 2014; Zhong and Zhao, 2014). The increase of surface stress indicates the intensification of the upper ocean circulation as well as the increase roughness of sea ice bottom (Tsamados et al., 2014). An interesting phenomenon in our results is that at some stations that the surface stress increases dramatically although both the sea ice retreat and the wind stress decrease, i.e., the surface stress is high-

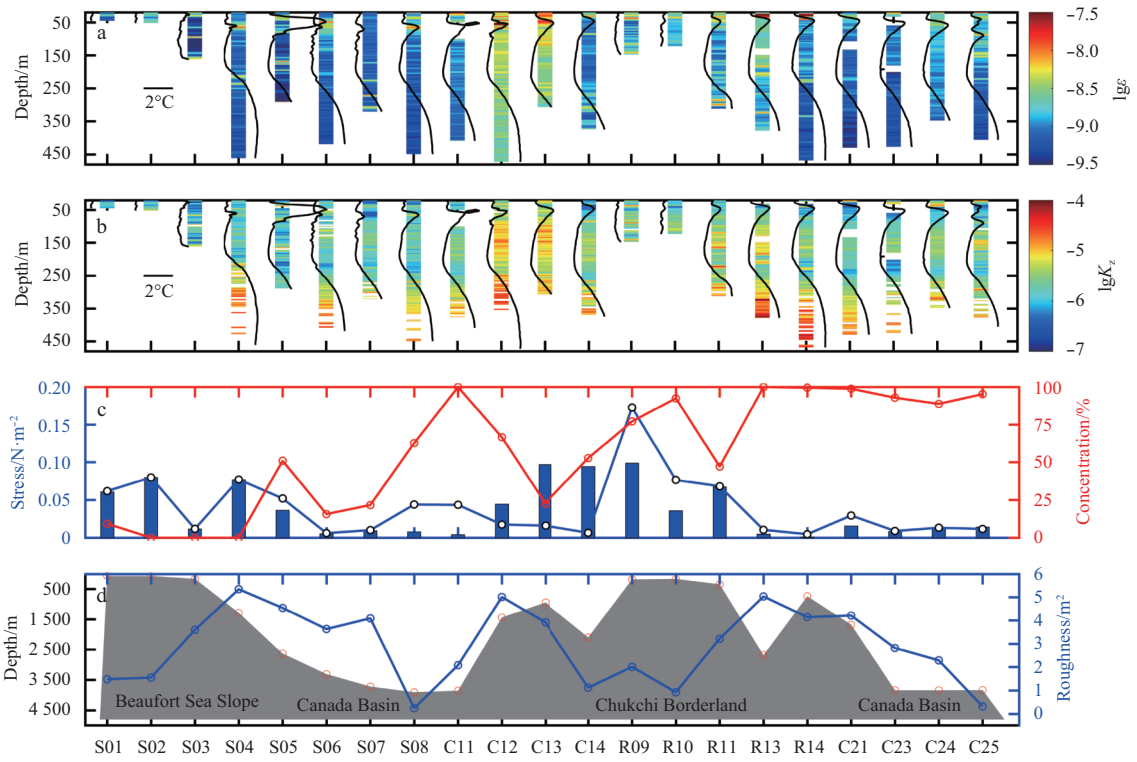

Fig. 3. Parameters at different stations. a. The turbulent dissipation rate (ε, W/kg); b. diapycnal diffusivity (K_z, m^2/s); c. the wind stress (blue dot-line), the surface stress (blue bar) and the sea ice concentration (red dot-line) of the corresponding stations; and d. depth of water (shaded gray, m) and bottom roughness (blue dot-line, $\log_{10}$ (roughness), m^2) for each station. The vertical black curve line represents the temperature profiles of each station in Figs 3a and b, the scale is shown in the horizontal black line.

er than the wind stress at Stas C12, C13 and C14. This indicates that the sea ice motion is dominated in the final results of the total surface stress due to the strengthening of sea ice movement. Stas C12 and C13 show a consistent strong mixing at all depth. These two stations located at the sea ice edge where the sea ice motion is stronger. The periodical change of surface stress could induce near-inertial internal waves which in turn contribute to the increase of vertical mixing.

The complex and steep topography of the Chukchi Borderland region not only divert the flows pathway of AW but also has a great impact on its vertical mixing. Stas S04, C12 and R13 have relatively high topography roughness and relatively high mixing comparing with their adjacent stations (Figs 3a and d). However, no significant correlation coefficient is found between the turbulent dissipation rate and the topography. We will discuss these further in details in the next section.

The main area of AW's heat dissipation is in the Chukchi Borderland region where the turbulent dissipation rate can be in the range of 1.27×10^{-9}– 3.31×10^{-9} W/kg (Fig. 4a). While it is in the range of 6.63×10^{-10}– 1.09×10^{-9} W/kg in the eastern Chukchi Borderland (Fig. 4a). The minimum turbulent dissipation rate appears in the southwestern part of the basin that in the range of 4.60×10^{-10}– 1.06×10^{-9} W/kg. These average dissipation rate close to (but above) the instrument noise level and comparable to previous studies (Lenn et al., 2009; Guthrie et al., 2013; Rippeth et al., 2015). The dissipation rate is relatively small in the south-western Canada Basin (Sta. S04 is located in the Beaufort Sea slope and is an exception with the relatively high dissipation rate of 1.33×10^{-9} W/kg) while it is relatively high in the Chukchi Borderland. A noteworthy evidence is that Stas C23 to C25 (located in the western basin) show an overall relatively high dissipation rate. These stations are located just at the mouth of thermohaline intrusions area of AW. The average of diapycnal diffusivity is 4.84×10^{-6} m^2/s with a maximum of 1.46×10^{-5} m^2/s (Fig. 4b).

We calculated the vertical heat flux based on the diapycnal diffusivity and the gradient of temperature. The typical vertical heat flux above AW (200–300 m) is less than 0.35 W/m^2 around Chukchi Borderland and its adjacent region (Fig. 5). The minimum heat flux is at Sta. S05 with a value of 0.095 W/m^2 in the southwestern basin and a maximum of 0.712 W/m^2 at Sta. C12 at the Northwind Ridge. The average of the heat flux is 0.27 W/m^2 which also in consistent with the previous observation (i.e., Timmermans et al., 2008; Guthrie et al., 2013; Rippeth et al., 2015). The heat content of Sta. C23 in 200–600 m is larger than that at Stas C24 and C25 (Fig. 2c) while its heat flux is small comparing with Stas C24 and C25 (Fig. 5). This discrepancy would favour the maintenance of AW heat near the Northwind Ridge and the further transport of this warm signal down to the south. The temperature of AW core at Sta. C23 is higher than that of the other stations along this Section C which indicates that it is located in the core of AW that flows along the Northwind Ridge. The relatively weak dissipation rate and vertical shear of the geostrophic current (Fig. 7 in the next section) results in this relatively small vertical heat flux at Sta. C23.

3.3 *Factors that regulate the mixing environment*

From the previous section, it is clear that down to the depth of AW there is a significant increase in the turbulent dissipation rate. In this section, we will discuss different factors that contribute to the mixing above the AW which includes: the near-inertial waves, the steep topography, the tidal kinetic energy and eddies. Only Sta. TU1 captures a cold eddy and this factor is excluded in

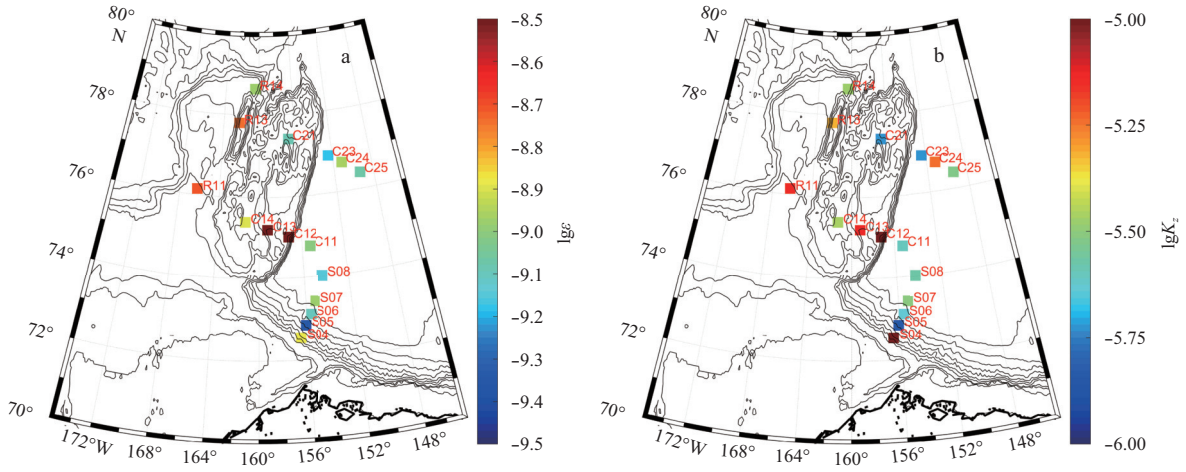

Fig. 4. The average turbulent dissipation rate (W/kg) (a) and diapycnal diffusivity (m^2/s) in 200–300 m above AW (b).

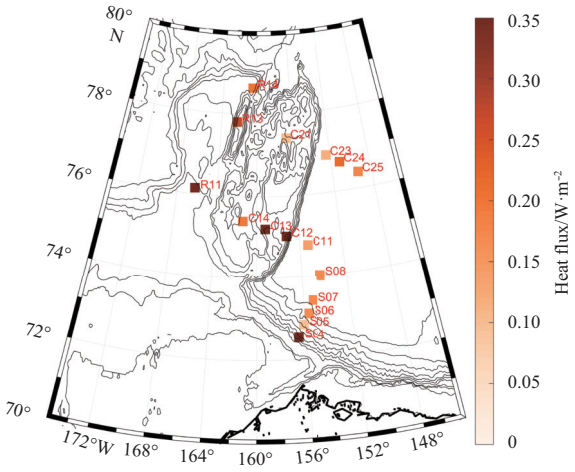

Fig. 5. The average of the vertical heat flux in 200–300 m above AW.

our present analysis. We will evaluate the rest of factors to determine their contribution to the heat release of AW and the dominate factors. As it is stated in our previous discussion, the sea ice acts as a barrier to the wind that imposed on the sea surface. Here we adopted Yang's (2009) methods to calculate the surface stress (considering the sea ice concentration and sea ice motion) in order to evaluate the potential effects of the near-inertial waves that may contribute to the mixing.

The presence of sea ice would significantly inhibit the wind-induced energy into the ocean. However, as the dramatic decline of sea ice continues and the corresponding increase of surface stress, the upper ocean responses to the wind forcing more readily and this leads to the generation of stronger near-inertial waves and thus increases the mixing to some extent (Rainville and Woodgate, 2009). However, our results show that there is no significant correlation between the turbulent dissipation rate and the surface stress for these stations (figure not shown). Obviously, there are something else beyond this relationship. The upper ocean becomes more stratified when the sea ice melt and this would inhibit the development of near-inertial waves and thus the wind-induced mixing (Guthrie et al., 2013). In a recent study by Lincoln et al. (2016), they revealed that there is no significant change of mixing in the intermediate depths in the interior of the Canada Basin due to the increasing stratification. In addition to that there is also no clear correlation between the topography roughness and the dissipation rate (figure not shown). After evaluating different factors that may contribute to the mixing, we found that the tidal kinetic energy has a relatively strong correlation with the dissipation rate in the layer of 200–300 m (Fig. 6). The tidal kinetic energy is strong in the shallow Chukchi Sea, the Chukchi Borderland region and western Beaufort Sea. Those tides which interact with the rough topography may significantly contribute to the mixing.

Another important contribution might comes from the BG. The Chukchi Borderland and its adjacent region are special for they subjected to the influence of the BG (a large scale anticyclonic circulation in the Canada Basin). The intensity of BG regulates the accumulation and release of freshwater (Proshutinsky et al., 2009) and further on the vertical strength of stratification. Whether the regional difference in stratification that induced by BG is contributing to the regional differences in vertical turbulent mixing remains a question. In order to address this question, based on the thermal wind relationship we calculated the vertical shear of geostrophic current between adjacent stations (the magnitude of this value could be used to evaluate the effects of BG on each station regarding their distances to the BG center) (Fig. 7a). Our research survey stations covered a large area with stations inside and outside the BG. Comparing Figs 3 with 7a, relatively consistent spatial distribution between the vertical shear of geostrophic current and the dissipation rate is revealed, i.e., stronger vertical shear of geostrophic current corresponds to stronger dissipation rate like Stas R11 and R13, Stas C24 and C25. This is an important enlightenment for us that the regional differences in turbulent mixing to some extent may relates to the intensity and shifting position of the BG. Both the Section S and two C sections are located at the edge of BG (Fig. 7b) where both the geostrophic current and the vertical shear are strong on section S in the south-western basin. While the overall geostrophic current and vertical shear in northern Section C are smaller than the southern Section C. Those stations that north of the Chukchi Borderland (far away from the periphery of BG), the vertical shear of geostrophic current is reduced, e.g., Stas R13 and R14 where the dissipation rate is also relatively small. However, the linear relationship between the vertical shear of geostrophic current and the turbulent dissipation rate is not significant as some stations were largely controlled by the tidal kinetic energy and the topo-

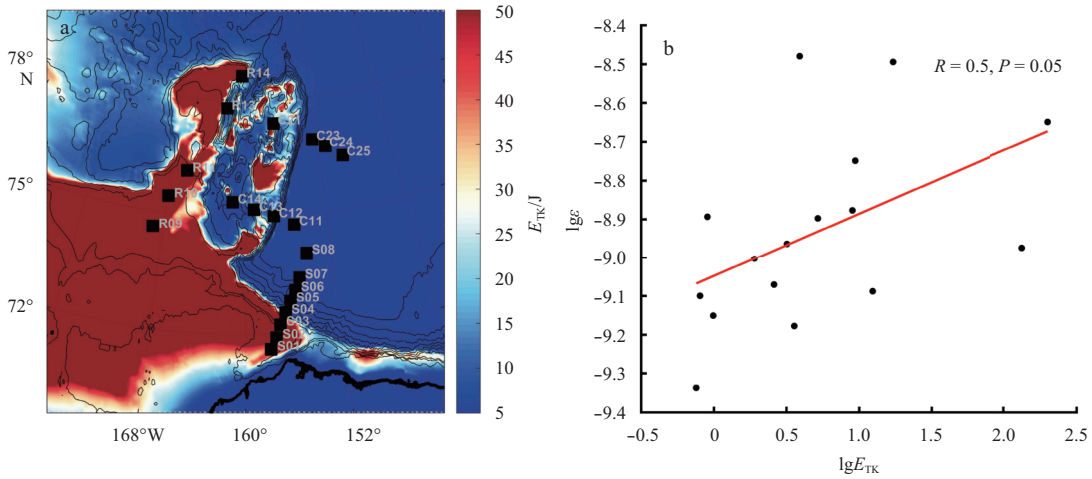

Fig. 6. Tidal Kinetic Energy and depth averaged turbulent dissipation rate. a. Tidal Kinetic Energy above 300 m considering the M_2, S_2, K_1 and O_1 tides; and b. the turbulent dissipation rate average in the depth range of 200–300 m (ε, W/kg) vs tidal kinetic energy (E_{TK}, J) above 300 m, 16 VMP profiles with depth larger than 200 m were used in this comparison.

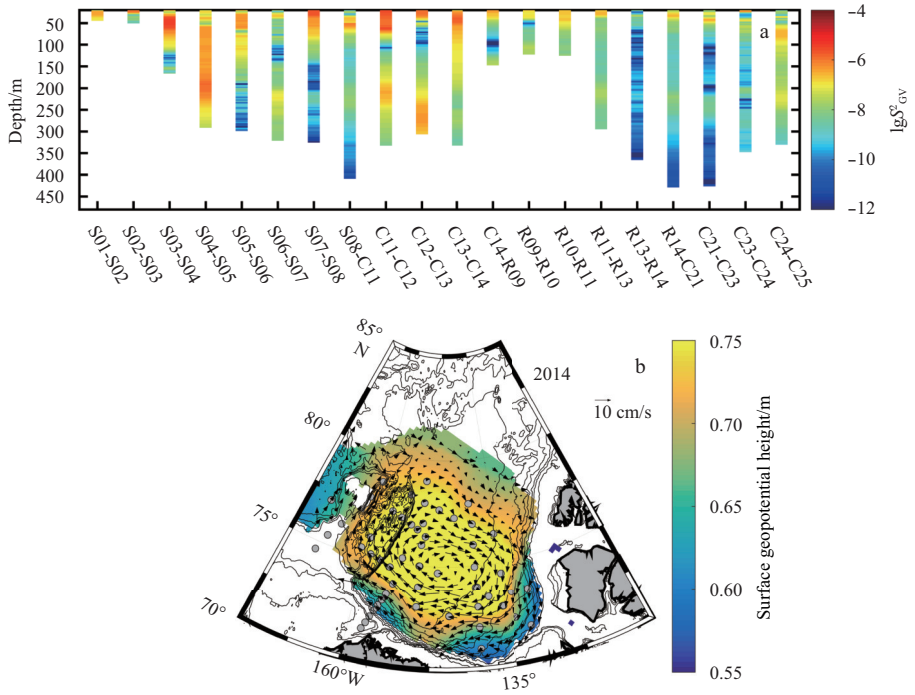

Fig. 7. Vertical shear of the geostrophic current between two adjacent stations (a) and surface geopotential height (shaded, with units of geopotential meters) and geostrophic currents (vectors) relative to 10 MPa (b).

graphy roughness. So the results of Fig. 7 are more of an implication for the potential impacts of BG.

4 Regional difference with/without the double-diffusive convection regime

There are two mechanisms that controlling the vertical mixing right above AW, i.e., the double-diffusive convection and the instability of turbulent shear. In order to evaluate the vertical heat flux of the double-diffusive convection regime, the laboratory parameterized method and the direct calculation based on the vertical temperature gradient and diapycnal diffusivity is used for comparison (for each right subplot of each station in Fig. 8). The laboratory parameterized method is a universal method to evaluate the heat flux of double-diffusive convection in the Arctic Ocean where the direct microstructure observation is sparse. So the purpose of this comparison is to validate this parameterized method with the direct observed results. The former method simply considers the effect of double-diffusive convection while the latter method considers the combined effects of both mechanisms. The formulation of the parameterized method (Kelley, 1990) of double-diffusive convection is

$$F_H = 0.003\ 2e^{(4.8/R_\rho^{0.72})}\rho c_p\left(\frac{\alpha g \kappa_T^2}{\nu}\right)^{1/3}(\Delta T)^{4/3},$$

where the density ratio is $R_\rho = (\beta\delta S)/(\alpha\delta\theta)$, $\alpha = -\rho^{-1}\partial\rho/\partial\theta$ is

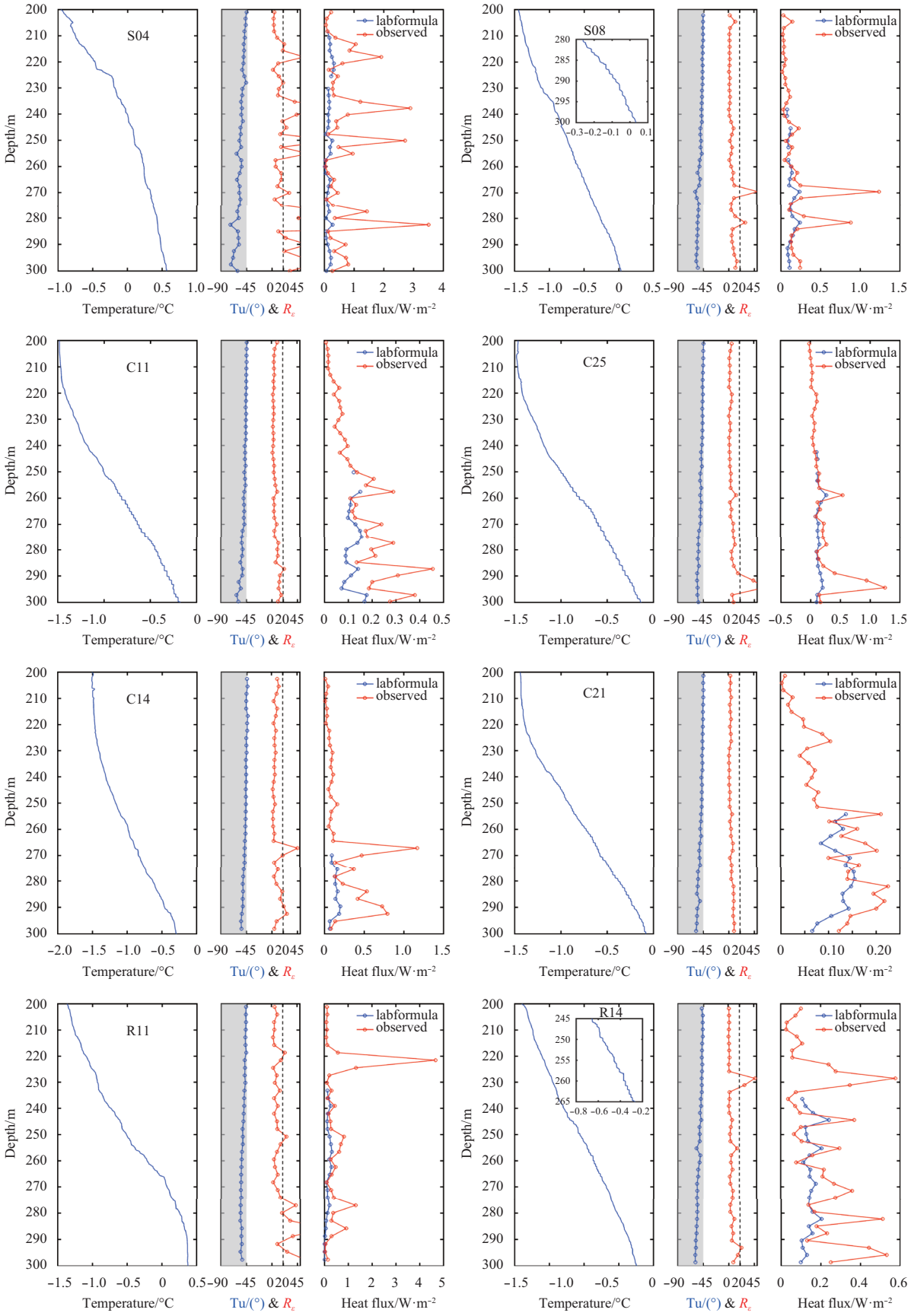

Fig. 8. Comparison between the stations with/without the double-diffusive convection regime. For each station from left to right, temperature (blue line), Turner angle (blue dot-line) and buoyancy Reynolds number (red dot-line), and the laboratory formula calculation of heat flux (Kelley, 1990) vs direct observation from VMP (red dot-line).

the thermal expansion coefficient, $v=1.8\times10^{-6}\,\mathrm{m^2/s}$ is the kinematic viscosity, $\kappa_T=1.4\times10^{-7}\,\mathrm{m^2/s}$ is the molecular diffusivity for heat, g is the gravitational acceleration and the thermal step ΔT is estimated from the layer height H using $\Delta T = <\partial\theta/\partial z>H$ (Robertson, 1999). We estimated the layer height from the large scale stratification parameters using the relationship proposed by Kelley (1984):

$$H=\left[0.25\times10^{9}R_{\rho}^{1.1}vk_T^{-1}(R_{\rho}-1)\right]^{0.25}\sqrt{k_T\langle N^{-1}\rangle}.$$

Studies have shown a close relationship between the presence of double-diffusive convection regime and the background mixing environment (e.g., Lenn et al., 2009; Fer, 2009). The buoyancy Reynolds number is calculated to evaluate the relationship between the turbulent dissipation rate and the halocline (the red line in each middle subplot of each station in Fig. 8). The turbulent effect significantly dominates (turbulent overwhelms the effects of stratification) when the buoyancy Reynolds number larger than 20 (Yamazaki, 1990).

The weak turbulent mixing above the AW interface is benefit for the appearance of double-diffusive staircase regime between the warm and salty AW and cold and fresh Pacific Water. The absence of double-diffusive convection regime to some extent would allow the wind induced near-inertial waves permeate into the depth of AW and interact with AW that results in greater heat release to the upper ocean (Ghaemsaidi et al., 2016). There are eight stations out of the 21 VMP-deployed stations were detected with double-diffusive staircase structure (for each left subplot of each station in Fig. 8), i.e., S07, S08, C11, C25, C24, C23, C21 and R14. There are a small part of weak double-diffusive staircase structure appears in the depth of 200–300 m at S07, S08 and R14. At those stations with the double-diffusive staircase structure, the profile of the Turner angle (Thorpe, 2005) is in the criterion of –90°<*Tu*<–45°, e.g., C11, C25 and R14. There are also some stations the Turner angle fells in this criteria range but has no double-diffusive staircase structure, e.g., S04, C14 and R11. In fact, two criteria are needed for the formation of double-diffusive staircase structure. One is the Turner angle, the other is the buoyancy Reynolds number which should be smaller than 20. For instance, the buoyancy Reynolds number is mostly larger than 20 at Sta. S04 although its Turner angle meets the criterion. The relatively weak stratification promotes the development of turbulent mixing and thus disrupt the formation of double-diffusive staircase.

In those eight stations that have double-diffusive staircase structure, the vertical scale of the staircase is ~3 m. This structure is not regional restricted to the Canada Basin, Sta. C21 in the Northwind Ridge and Sta. R14 in the Chukchi Rise also have the double-diffusive staircase. Most of the heat flux of the double-diffusive staircase fells in the range of ~0.1–0.2 W/m^2. The VMP observation captured a lot of subtle variability of heat flux. Large discrepancy appears between the direct calculation from VMP observation and the parameterized method when the buoyancy Reynolds number is larger than 20 and an absence of double-diffusive staircase structure. This indicates that the absence of double-diffusive staircase above the AW (where cold and fresh water above warm and salty water) is related to the relatively strong vertical shear. It is also show a validation of using parameterized method to estimate the vertical heat flux of double-diffusive staircase structure. The direct observation of turbulent vertical heat flux is frequently larger than 1 W/m^2. This direct observation result is more of an instant situation rather than a mean situation. Overall, the vertical heat flux of AW remains in a relatively weak situation.

5 Discussion and conclusions

We analyzed the turbulent mixing above the AW around the Chukchi Borderland and its adjacent region based on the direct observation from 2014 summer research cruise. The surface wind becomes more efficient in driving the upper ocean movement in a rapid decline period of sea ice, thus results in a more restless interior of Arctic Ocean. The increase mobility of sea ice and the increase of surface stress exert stronger forcing to the upper ocean and this to some extent could induce the formation of near-inertial waves that promote the vertical mixing. The variabilities of surface forcing (surface stress) are contributing to the formation of near-inertial waves. In this study, based on our present data the surface stress is calculated as a proxy of the potential effects of near-inertial waves. There is no significant relationship between the turbulent mixing above the AW and the surface stress. Our results show a significant correlation between the tidal kinetic energy and the dissipation rate at the depth of 200–300 m which indicate that the tidal kinetic energy dominates the mixing at this layer. Beside this, no significant correlation is found with the other factors like wind and topography. The extent and strength of BG will alter the intensity of vertical shear of geostrophic current and further might contribute to the regional differences of turbulent mixing above the AW. But this needs further investigation to confirm it which includes a wider microstructure observation around the BG. On the other hand, the deepening of AW could also change the vertical gradient of temperature and thus the vertical heat flux (Zhong and Zhao, 2014). By analysing the direct microstructure observation, the regional difference of turbulent mixing between the continental shelf and the basin is given. At the periphery of the southwestern Canada Basin where the continental shelf with water depth <2 000 m (the buoyancy Reynolds number is larger than 20), the relatively strong turbulent mixing is dominated and the double-diffusive staircase structure is absent. While in the interior Canada Basin and some parts of the Chukchi Borderland where it is dominated by the warm AW, the overall buoyancy Reynolds number is smaller than 20 that supports the maintenance of double-diffusive staircase structure.

The double-diffusive staircase structure is covering from north of Chukchi Borderland to the interior Canada Basin. In those regions with the double-diffusive staircase structure the parameterized method is a good approximation to evaluate the vertical heat flux while this method fell to estimate the real vertical heat flux in other situation. The average heat flux above the AW in the Chukchi Borderland and its adjacent region is 0.27 W/m^2 with the highest appears in the north of Northwind Ridge. In the layer of 200–300 m above the AW, the dissipation rate is 4.60×10^{-10}–3.31×10^{-9} W/kg (1.33×10^{-9} W/kg for average) while the diapycnal diffusivity is 1.45×10^{-6}–1.46×10^{-5} m^2/s (4.84×10^{-6} m^2/s for average).

A noticeable evidence is for those stations with the surface stress larger than the wind stress (located at the marginal sea ice zone), a clear relatively strong background mixing is shown from the depth of 20 m to AW (~400 m) with the diapycnal diffusivity $K_z>10^{-5.5}$ m^2/s. This is contrast to the resent study (Lincoln et al., 2016) which reveals there is no significant change of mixing in the intermediate depths in the interior of Canada Basin due to the increasing stratification. While in our study region where the stations are located in the marginal sea ice zone, the increase of

surface stress would make a difference. More heat energy would release from the AW to the upper layer due to this stronger turbulent mixing. This indicates the wind could be more efficient for mixing in the marginal sea ice zone.

Acknowledgements

The authors thank the research groups of the 6th Chinese Arctic research expedition for assistant of collecting the CTD and turbulent microstructure data. Parts of the hydrographic data are from the Beaufort Gyre Exploration Project (BGEP) at http://www.whoi.edu/beaufortgyre/. The ECMWF surface wind data are available at https://www.ecmwf.int/en/forecasts/datasets. The sea ice velocity is distributed by NSIDC (https://nsidc.org/data/nsidc-0116). The sea ice concentration data is downloaded from https://seaice.uni-bremen.de/sea-ice-concentration/#Data_Archive. The data of the Arctic Ocean Dynamics-based Tide Model is from http://polaris.esr.org/ptm_index.html.

References

Carmack E C, Macdonald R W, Perkin R G, et al. 1995. Evidence for warming of Atlantic water in the southern Canadian Basin of the Arctic Ocean: results from the Larsen-93 expedition. Geophys Res Lett, 22(9): 1061–1064

D'Asaro E A, Morison J H. 1992. Internal waves and mixing in the Arctic Ocean. Deep-Sea Res: A, 39: S459–S484

Dee D P, Uppala S M, Simmons A J, et al. 2011. The ERA-Interim reanalysis: configuration and performance of the data assimilation system. Quart J Roy Meteor Soc, 137(656): 553–597, doi: 10.1002/qj.828

Dosser H V, Rainville L, Toole J M. 2014. Near-inertial internal wave field in the Canada Basin from ice-tethered profilers. J Phys Oceanogr, 44(2): 413–426, doi: 10.1175/JPO-D-13-0117.1

Dosser H V, Rainville L. 2016. Dynamics of the changing near-inertial internal wave field in the Arctic Ocean. J Phys Oceanogr, 46(2): 395–415

Egbert G D, Erofeeva S Y. 2002. Efficient inverse modeling of barotropic ocean tides. J Atmos Oceanic Technol, 19(2): 183–204

Fer I. 2009. Weak vertical diffusion allows maintenance of cold halocline in the central Arctic. Atmos Oceanic Sci Lett, 2(3): 148–152

Ghaemsaidi S J, Dosser H V, Rainville L, et al. 2016. The impact of multiple layering on internal wave transmission. J Fluid Mech, 789: 617–629

Guthrie J D, Morison J H, Fer I. 2013. Revisiting internal waves and mixing in the Arctic Ocean. J Geophys Res, 118(8): 3966–3977

Ivey G N, Winters K B, Koseff J R. 2008. Density stratification, turbulence, but how much mixing?. Annu Rev Fluid Mech, 40(1): 169–184

Kaneko H, Yasuda I, Komatsu K, et al. 2012. Observations of the structure of turbulent mixing across the Kuroshio. Geophys Res Lett, 39(15): L15602, doi: 10.1029/2012GL052419

Kelley D. 1984. Effective diffusivities within oceanic thermohaline staircases. J Geophys Res, 89(C6): 10484–10488, doi: 10.1029/JC089iC06p10484

Kelley D E. 1990. Fluxes through diffusive staircases: a new formulation. J Geophys Res, 95(C3): 3365–3371

Kikuchi T, Inoue J, Morison J H. 2005. Temperature difference across the Lomonosov Ridge: implications for the Atlantic Water circulation in the Arctic Ocean. Geophys Res Lett, 32(20): L20604, doi: 10.1029/2005GL023982

Lenn Y D, Wiles P J, Torres-Valdes S, et al. 2009. Vertical mixing at intermediate depths in the Arctic boundary current. Geophys Res Lett, 36(5): L05601, doi: 10.1029/2008GL036792

Lincoln B J, Rippeth T P, Lenn Y D, et al. 2016. Wind-driven mixing at intermediate depths in an ice-free Arctic Ocean. Geophys Res Lett, 43(18): 9749–9756, doi: 10.1002/2016GL070454

Martin T, Steele M, Zhang J L. 2014. Seasonality and long-term trend of Arctic Ocean surface stress in a model. J Geophys Res, 119(3): 1723–1738

McLaughlin F, Shimada K, Carmack E, et al. 2005. The hydrography of the southern Canada Basin, 2002. Polar Biol, 28(3): 182–189, doi: 10.1007/s00300-004-0701-6

McLaughlin F A, Carmack E C, Williams W J, et al. 2009. Joint effects of boundary currents and thermohaline intrusions on the warming of Atlantic water in the Canada Basin, 1993-2007. J Geophys Res, 114(C1): C00A12, doi: 10.1029/2008JC005001

Osborn T. R 1980. Estimates of the local rate of vertical diffusion from dissipation measurements. J Phys Oceanogr, 10: 83–89

Padman L, Dillon T M. 1987. Vertical heat fluxes through the Beaufort Sea thermohaline staircase. J Geophys Res, 92(C10): 10799–10806

Padman L, Dillon T M. 1991. Turbulent mixing near the Yermak Plateau during the Coordinated Eastern Arctic Experiment. J Geophys Res, 96(C3): 4769–4782

Padman L, Erofeeva S. 2004. A barotropic inverse tidal model for the Arctic Ocean. Geophys Res Lett, 31(2): L02303, doi: 10.1029/2003GL019003

Polyakov I V, Alekseev G V, Timokhov L A, et al. 2004. Variability of the intermediate Atlantic water of the Arctic Ocean over the last 100 years. J Climate, 17(23): 4485–4497

Polyakov I V, Alexeev V A, Ashik I M, et al. 2011. Fate of early 2000s arctic warm water pulse. Bull Amer Meteor Soc, 92(5): 561–566, doi: 10.1175/2010BAMS2921.1

Polyakov I V, Timokhov L A, Alexeev V A, et al. 2010. Arctic Ocean warming contributes to reduced polar ice cap. J Phys Oceanogr, 40(12): 2743–2756, doi: 10.1175/2010JPO4339.1

Polyakov I V, Pnyushkov A V, Timokhov L A. 2012. Warming of the intermediate Atlantic water of the Arctic Ocean in the 2000s. J Climate, 25(23): 8362–8370

Proshutinsky A, Krishfield R, Timmermans M L, et al. 2009. Beaufort Gyre freshwater reservoir: state and variability from observations. J Geophys Res, 114(C1): C00A10, doi: 10.1029/2008JC005104

Rainville L, Lee C M, Woodgate R A. 2011. Impact of wind-driven mixing in the Arctic Ocean. Oceanography, 24(3): 136–145, doi: 10.5670/oceanog.2011.65

Rainville L, Winsor P. 2008. Mixing across the Arctic Ocean: microstructure observations during the Beringia 2005 Expedition. Geophys Res Lett, 35(8): L08606, doi: 10.1029/2008GL033532

Rainville L, Woodgate R A. 2009. Observations of internal wave generation in the seasonally ice-free Arctic. Geophys Res Lett, 36(23): L23604, doi: 10.1029/2009GL041291

Rippeth T P, Lincoln B J, Lenn Y D, et al. 2015. Tide-mediated warming of Arctic halocline by Atlantic heat fluxes over rough topography. Nat Geosci, 8(3): 191–194

Robertson R. 1999. Mixing and heat transport mechanisms in the upper ocean in the Weddell Sea [dissertation]. Corvallis: Oregon State University

Shimada K, Kamoshida T, Itoh M, et al. 2006. Pacific Ocean inflow: influence on catastrophic reduction of sea ice cover in the Arctic Ocean. Geophys Res Lett, 33(8): L08605, doi: 10.1029/2005GL025624

Shimada K, McLaughlin F, Carmack E, et al. 2004. Penetration of the 1990s warm temperature anomaly of Atlantic Water in the Canada Basin. Geophys Res Lett, 31(20): L20301, doi: 10.1029/2004GL020860

Spreen G, Kaleschke L, Heygster G. 2008. Sea ice remote sensing using AMSR-E 89-GHz channels. J Geophys Res, 113(C2): C02S03, doi: 10.1029/2005JC003384

Thorpe S A. 2005. The Turbulent Ocean. Cambridge, UK: Cambridge University Press

Timmermans M L, Toole J, Krishfield R, et al. 2008. Ice-Tethered Profiler observations of the double-diffusive staircase in the Canada Basin thermocline. J Geophys Res, 113(C1): C00A02, doi: 10.1029/2008JC004829

Tsamados M, Feltham D L, Schroeder D, et al. 2014. Impact of variable atmospheric and oceanic form drag on simulations of Arctic sea ice. J Phys Oceanogr, 44(5): 1329–1353

Tschudi M C, Fowler J, Maslanik, et al. 2016. Polar Pathfinder Daily 25 km EASE-Grid Sea Ice Motion Vectors, Version 3. Boulder,

Colo: National Snow and Ice Data Center
Turner J S. 2010. The melting of ice in the Arctic Ocean: the influence of double-diffusive transport of heat from below. J Phys Oceanogr, 40(1): 249–256, doi: 10.1175/2009JPO4279.1
Woodgate R A, Aagaard K, Swift J H, et al. 2005. Pacific ventilation of the Arctic Ocean's lower halocline by upwelling and diapycnal mixing over the continental margin. Geophys Res Lett, 32(18): L18609, doi: 10.1029/2005GL023999
Woodgate R A, Aagaard K, Swift J H, et al. 2007. Atlantic water circulation over the Mendeleev Ridge and Chukchi Borderland from thermohaline intrusions and water mass properties. J Geophys Res, 112(C2): C02005, doi: 10.1029/2005JC003416
Yamazaki H. 1990. Stratified turbulence near a critical dissipation rate. J Phys Oceanogr, 20(10): 1583–1598
Yang Jiayan. 2009. Seasonal and interannual variability of downwelling in the Beaufort Sea. J Geophys Res, 114(C1): C00A14, doi: 10.1029/2008JC005084
Zhao Jinping, Gao Guoping, Jiao Yutian. 2005. Warming in Arctic intermediate and deep waters around Chukchi Plateau and its adjacent regions in 1999. Sci China: Ser D. Earth Sci, 48(8): 1312–1320
Zhong Wenli, Zhao Jinping. 2014. Deepening of the Atlantic Water core in the Canada Basin in 2003-11. J Phys Oceanogr, 44(9): 2353–2369, doi: 10.1175/JPO-D-13-084.1
Zhong Wenli, Zhao Jinping, Shi Jiuxin, et al. 2015. The Beaufort Gyre variation and its impacts on the Canada Basin in 2003-2012. Acta Oceanol Sin, 34(7): 19–31, doi: 10.1007/s13131-015-0657-0